Experimental demonstration of real-time adaptive one-qubit quantum-state tomography

Qi Yin, Li Li, Xiao Xiang, Guo-Yong Xiang,* Chuang-Feng Li, and Guang-Can Guo
Key Laboratory of Quantum Information, University of Science and Technology of China, Chinese Academy of Sciences, Hefei 230026, People's Republic of China
and Synergetic Innovation Center of Quantum Information and Quantum Physics, University of Science and Technology of China, Hefei 230026, People's Republic of China
(Received 11 August 2016; published 20 January 2017)

Quantum-state tomography plays a pivotal role in quantum computation and information processing. To improve the accuracy in estimating an unknown state, carefully designed measurement schemes, such as adopting an adaptive strategy, are necessarily needed, which have gained great interest recently. In this work, based on the proposal of Sugiyama *et al.* [Phys. Rev. A **85**, 052107 (2012)], we experimentally realize an adaptive quantum-state tomography for one qubit in an optical system. Since this scheme gives an analytical solution to the optimal measurement basis problem, our experiment is updated in real time and the infidelity between the real state and the estimated state is tracked with the detected photons. We observe an almost $1/N$ scaling rule of averaged infidelity against the overall number of photons, N, in our experiment, which outperforms $1/\sqrt{N}$ of nonadaptive schemes.

DOI: 10.1103/PhysRevA.95.012129

I. INTRODUCTION

Quantum-state tomography is a process to experimentally characterize the state of any given quantum system and has been widely applied in quantum computation and information processing [1–3]. Usually, an ensemble of identical copies of the targeted states is prepared and then passed through different measurement settings. Based on the collected data, one can reconstruct the state with the help of certain classical algorithms [4–6]. Nevertheless, with limited resources the quantum state can only be estimated up to certain accuracy; thus, the problem to improve accuracy in estimating an unknown state has always attracted lots of attention [6–13]. For a qubit system, the traditional way is to fix several measurement bases prior to the experiment and then reconstruct the density matrix based on the measurement results [6], whose estimation error scales with the number of copies, N, as $1/\sqrt{N}$ for pure and nearly pure states [7,8]. By choosing some special measurement basis, such as a mutually unbiased basis (MUB) or cubelike basis [9–11], the prefactor of the scaling rule can be improved, but the power-law index of N is scarcely changed. In fact, it has been shown that the estimation error scaling rule is bounded by $1/N$, and theoretically it can be achieved by employing a collective measurement strategy, i.e., by measuring in the huge Hilbert space of $\rho^{\otimes N}$ [12,13]. However, it is impossible to experimentally implement collective measurements with current technology. An alternative solution is to employ an adaptive strategy: rather than using the fixed basis, this scheme changes the next measurement setting based on previous measurement settings and outcomes. As a result, the performance of quantum-state tomography can be improved remarkably and can even approach the estimation limit [14,15].

In adaptive quantum-state tomography, the measurement basis is continuously updated with the collected data based on some criterion, such as maximizing the mean expected fidelity or Fisher information [14,16], or according to the Bayesian inference [17,18]. However, all these proposals are highly computationally intensive and the involved optimization problem becomes intractable after dozens of trials, which makes them infeasible for realistic experimental implementations. Recently, several efficient adaptive schemes have been proposed [19–22], which took different strategies for quantum-state tomography and achieved better performance in numerical simulations or experiments. Here we report an experimental realization of adaptive quantum-state tomography proposed by Sugiyama *et al.* [19]. This scheme, based on average-variance optimality [23], has an analytic solution to the optimal measurement basis for the one-qubit case, which requires much less computational cost so that we can implement fast and real-time adaptive tomography experiments for very large N. The estimation accuracy, if infidelity is taken as the metric of the error, almost scales as $1/N$, approximating the theoretical limit.

II. ALGORITHM REVISED

In this section, we briefly review the main idea of this proposal [19]. A quantum measurement can be described by a positive operator-valued measure (POVM), $\Pi = \{\Pi_m\}_{m=1}^{M}$, with the probability of outcome m being observed given by Born's rule $p(m;\Pi|\rho) = \mathrm{Tr}(\Pi_m \rho)$. In quantum-state tomography, different sets of POVMs are required to fully reconstruct an unknown quantum state. Let $\Pi^n = \{\Pi_1, \Pi_2, \ldots, \Pi_n\}$ denote the sequence of chosen POVMs up to the nth trial in the adaptive procedure and $D^n = \{\Pi_{1,m_1}, \ldots, \Pi_{n,m_n}\} \in \mathcal{D}^n$ denote the corresponding outcome sequence obtained, where $\mathcal{D}^n$ represents the space of all possible outcome sequences. Here, we simplify the state in d-dimensional space as a vector $\boldsymbol{s} \in \mathbb{R}^{d^2-1}$ [24], i.e., $\rho = \rho(\boldsymbol{s})$. For instance, $\rho(\boldsymbol{s}) = \frac{1}{2}(\mathbf{1} + \boldsymbol{s}\cdot\boldsymbol{\sigma})$ in the one-qubit case, where $\boldsymbol{\sigma} = (\sigma_x, \sigma_y, \sigma_z)$ are the Pauli matrices. Then we obtain the following inequality for any estimator $\boldsymbol{s}^{\mathrm{est}}$ with N measurement trials:

$$\sum_{D^N \in \mathcal{D}^N} p(D^N|\boldsymbol{s})[\boldsymbol{s}^{\mathrm{est}}(D^N) - \boldsymbol{s}]^T H(\boldsymbol{s})[\boldsymbol{s}^{\mathrm{est}}(D^N) - \boldsymbol{s}] \geqslant \mathrm{Tr}[H(\boldsymbol{s})G(D^N, \boldsymbol{s}^{\mathrm{est}}, \boldsymbol{s})^T F(D^N, \boldsymbol{s})^{-1} G(D^N, \boldsymbol{s}^{\mathrm{est}}, \boldsymbol{s})], \quad (1)$$

*gyxiang@ustc.edu.cn

where

$$G(D^N,\boldsymbol{s}^{\rm est},\boldsymbol{s}) = \nabla_{\boldsymbol{s}} \sum_{D^N\in\mathcal{D}^N} p(D^N|\boldsymbol{s})\boldsymbol{s}^{{\rm est}T}(D^N), \tag{2}$$

$$F(D^N,\boldsymbol{s}) = \sum_{D^N\in\mathcal{D}^N} \frac{\nabla_{\boldsymbol{s}} p(D^N|\mathbf{s})\nabla_{\boldsymbol{s}}^T p(D^N|\boldsymbol{s})}{p(D^N|\boldsymbol{s})}, \tag{3}$$

$H(\mathbf{s})$ is a positive semidefinite matrix related to some error metric, and $F(D^N,\boldsymbol{s})$ is called the Fisher matrix. In fact, Eq. (1) is a generalization of the well-known Cramér-Rao inequality for quantum systems [19,25].

From now on, we need three approximations to derive the update criterion of the optimal measurement basis. As we can see, the right-hand side of Eq. (1) is the lower bound on variance of the estimator. When $N\to\infty$, the estimator converges to the true state and $G(D^N,\boldsymbol{s}^{\rm est},\boldsymbol{s})$ converges to the identity matrix I; it ends up with

$$K(D^N,\boldsymbol{s}) := {\rm Tr}[H(\boldsymbol{s})F(D^N,\boldsymbol{s})^{-1}]. \tag{4}$$

To simplify the inequality, now we consider this function $K(D^N,\boldsymbol{s})$ as the lower bound of the error. This is the first approximation, which has little effect on the accuracy especially when N is large. Then a natural thought is to choose a measurement update rule that minimizes the value of $K(D^N,\boldsymbol{s})$ so that we can possibly promote the estimation precision, which is exactly the guiding principle of the average variance optimality [23]. This can be formulated as the following optimization procedure after the nth trial has been finished:

$$\Pi_{n+1}^{\rm opt} = \arg\min_{\Pi_{n+1}\in\mathcal{M}} {\rm Tr}[H(\boldsymbol{s})F(D^{n+1},\boldsymbol{s})^{-1}], \tag{5}$$

where $\mathcal{M}$ is the set of possible measurement bases. Usually the calculation of a Fisher matrix requires summing over all possible measurement outcome sequences of all possible measurement basis sequences according to Eq. (3), which is an exponential amount of data and formidable to compute. To avoid this problem, here comes the second approximation: we only consider those measurement outcome sequences of the measurement basis sequence being performed in the current experiment instead of considering other possible measurement basis sequences:

$$F(D^{n+1},\boldsymbol{s}) \approx \tilde{F}(D^{n+1},\boldsymbol{s}|\Pi^{n+1}) = \sum_{i=1}^{n+1} F(\boldsymbol{\Pi}_i,\boldsymbol{s}), \tag{6}$$

where

$$F(\boldsymbol{\Pi}_i,\boldsymbol{s}) = \sum_{m_i=1}^{M} \frac{\nabla_{\boldsymbol{s}} p(m_i;\boldsymbol{\Pi}_i|\boldsymbol{s})\nabla_{\boldsymbol{s}}^T p(m_i;\boldsymbol{\Pi}_i|\boldsymbol{s})}{p(m_i;\boldsymbol{\Pi}_i|\boldsymbol{s})}. \tag{7}$$

Since the minimizing function depends on the unknown parameter $\boldsymbol{s}$ which is to be estimated, we adopt the last approximation to replace $\boldsymbol{s}$ with a randomly chosen initial value and then update it with the estimated $\boldsymbol{s}^{\rm est}(D^n)$ after every step. Finally, the update criterion is defined as

$$\Pi_{n+1}^{\rm opt} = \arg\min_{\Pi_{n+1}\in\mathcal{M}} {\rm Tr}\left[H\left(\boldsymbol{s}_n^{\rm est}\right)F\left(D^{n+1},\boldsymbol{s}_n^{\rm est}\right)^{-1}\right]. \tag{8}$$

This is in general a nonlinear minimization problem with high computational cost. In the one-qubit case, fortunately, an analytic solution can be derived. Let us denote the projective measurement basis of one qubit by

$$\Pi_{\pm}(\boldsymbol{a}) = \tfrac{1}{2}(\mathbf{1}\pm\boldsymbol{a}\cdot\boldsymbol{\sigma}), \tag{9}$$

where $\boldsymbol{a}$ is a vector on the Bloch sphere. Then the optimal basis given by Eq. (8) is

$$\boldsymbol{a}_{n+1}^{\rm opt} = \frac{B_n \boldsymbol{e}_{\rm min}(C_n)}{\|B_n \boldsymbol{e}_{\rm min}(C_n)\|}, \tag{10}$$

where

$$B_n = \sqrt{\tilde{F}\left(\boldsymbol{a}^n,\boldsymbol{s}_n^{\rm est}\right)H\left(\boldsymbol{s}_n^{\rm est}\right)^{-1}\tilde{F}_n\left(\boldsymbol{a}^n,\boldsymbol{s}_n^{\rm est}\right)}, \tag{11}$$

$$C_n = B_n\left[I-\hat{\boldsymbol{s}}_n^{\rm est}\boldsymbol{s}_n^{\rm estT}+\tilde{F}_n\left(\boldsymbol{a}^n,\boldsymbol{s}_n^{\rm est}\right)^{-1}\right]B_n, \tag{12}$$

and $\boldsymbol{e}_{\rm min}(C_n)$ is the eigenvector corresponding to the minimal eigenvalue of matrix C_n [19]. Thanks to the analytic solution, the computational cost of this proposal is extremely reduced, which makes it possible to implement adaptive quantum-state tomography for large N in experiments.

III. SIMULATIONS

In the one-qubit case, the traditional tomograph such as the MUB usually achieves different estimation precision for different states even with the same purity, i.e., the same length of the state vector in the Bloch sphere. For example, the expected infidelity scales as $1/\sqrt{N}$ for most of nearly pure states, whereas it scales as $1/N$ for the few states that are aligned with the measurement basis [21]. It is due to the asymmetry of information extraction when we apply a fixed measurement basis for different states. On the contrary, in adaptive schemes, we know from Eq. (8) that the measurement basis changes every step and is decided by the results achieved before, which are related to the target state (except for the first few ones which are chosen intentionally by researchers, here we fix $\sigma_x,\sigma_y,\sigma_z$ to be our first three measurements, which hardly affects the final estimate). So given the same update criterion for every state and the symmetry of the Bloch sphere, we claim when the measurement number is large enough, every state with the same purity will be reconstructed to the same precision with adaptive schemes in terms of average performance. Thus, instead of randomly choosing among all states, here we numerically simulate the performance of this adaptive tomography scheme for states with different r in the Bloch sphere, while (θ,ϕ) was fixed at $(\pi/4,\pi/4)$.

In Eq. (1), the matrix $H(\boldsymbol{s})$ is determined by which error metric is used to value the variance of the estimator, for instance, $H^{\rm HS}(\boldsymbol{s}) = \frac{1}{4}I$ for Hilbert-Schmidt (HS) distance and $H^{\rm IF}(\boldsymbol{s}) = \frac{1}{4}(I+\frac{\boldsymbol{s}\boldsymbol{s}^T}{1-\|\boldsymbol{s}\|^2})$ for infidelity (IF). Different expressions of $H(\boldsymbol{s})$ may lead to different results, so we would like to apply these two expressions in the update criterion to observe and compare the performance of the two slightly different adaptive tomography schemes. As depicted in Fig. 1, the average infidelity of both IF- and HS-based tomography decreases remarkably as N increases, except when N is too small ($N<50$), because the first and third approximations we made above are not quite suitable until N becomes sufficiently large. Then we fit a power law of the form $1-F\propto N^{\alpha}$ to these simulated data and found $\alpha=-0.99\pm0.04$, $-1.12\pm$

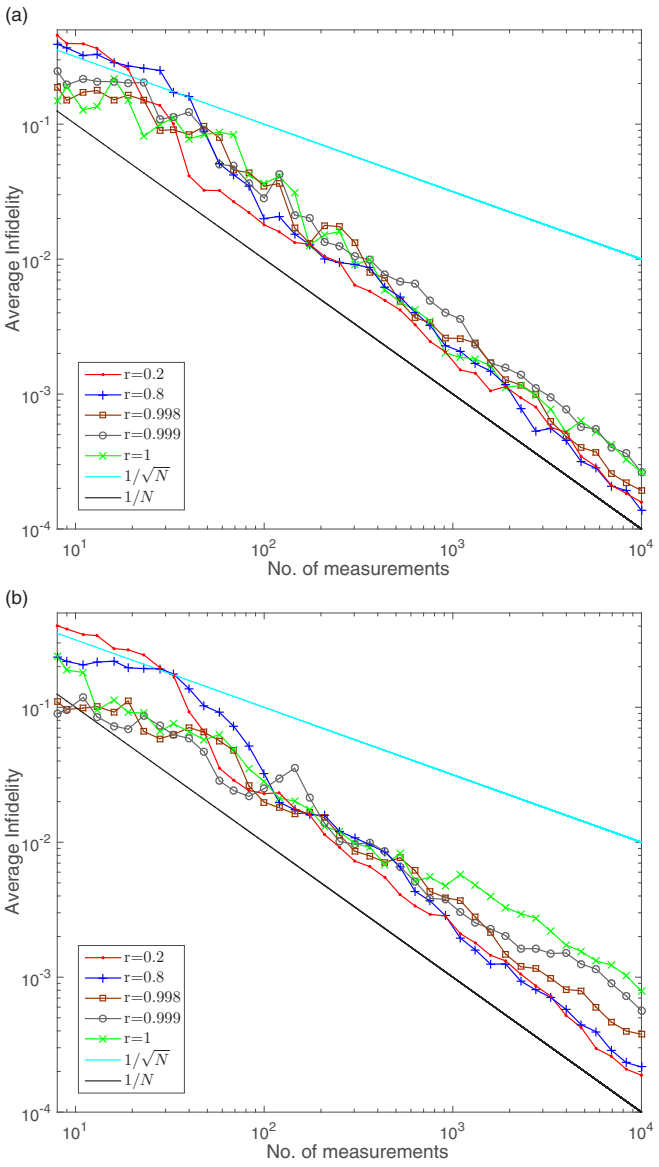

FIG. 1. Simulated average infidelity $1 - F(\hat{\rho},\rho)$ against number of measurements, N, for both adaptive tomography schemes: (a) IF-based tomography and (b) HS-based tomography. The true state is chosen with different $r = 0.2, 0.8, 0.998, 0.999$, and 1, while (θ,ϕ) is fixed at $(\pi/4,\pi/4)$. All the results presented here are the average of 20 independent runs. The cyan (upper) line of $1 - F = 1/\sqrt{N}$ and black (lower) line of function $1 - F = 1/N$ are shown for comparison.

0.05, -1.08 ± 0.04, -1.02 ± 0.04, and -1.07 ± 0.05 for IF-based tomography and $\alpha = -1.08 \pm 0.04, -1.11 \pm 0.04, -0.87 \pm 0.05, -0.80 \pm 0.06$, and -0.76 ± 0.07 for HS-based tomography in the sequence of $r = 0.2, 0.8, 0.998, 0.999, 1$. There is a small difference between the two schemes. The performance of IF-based tomography is almost the same for all states, while that of HS-based tomography becomes a little worse when r approaches 1, which is analyzed later. It should be noted that even the worst case of HS-based tomography, i.e., reconstructing the pure state, still outperforms the $1/\sqrt{N}$ scaling rule of nonadaptive schemes [9–11].

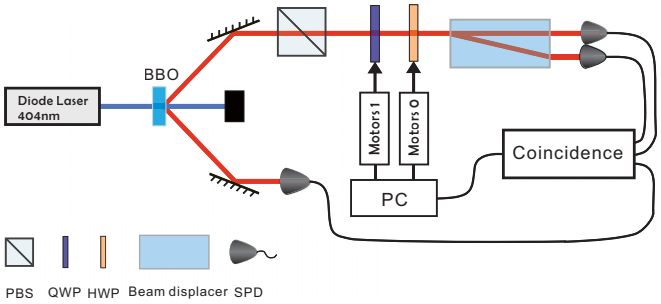

FIG. 2. Spontaneous parametric down-conversion is performed by pumping a nonlinear beta barium borate crystal with a 404-nm diode laser. One photon is sent directly to a detector as a trigger. The second photon is sent through a polarizer beam splitter to prepare it in a state of very pure horizonal polarization. The measurement basis is performed by a zero-order quarter-wave plate and a half-wave plate followed by a beam displacer, with two detectors collecting the photons. The wave plates are controlled by a computer to enable adaptation and driven by two step-motor stages.

IV. EXPERIMENTAL REALIZATION

Considering the pure state is the worst case for quantum-state estimation, without loss of generality, we have only experimentally implemented this adaptive tomography for a one-qubit pure state. In Fig. 2, by using type-I spontaneous parametric down-conversion in a nonlinear crystal, photon pairs are created. One of the photons is sent immediately to a single-photon counting module (SPCM) to act as a trigger. The second photon is sent through a polarizer beam splitter to prepare it in a state of very pure horizonal polarization. A zero-order quarter-wave plate and a half-wave plate followed by a beam displacer with high extinction ratio (more than 10 000:1) are used to project the photons onto any measurement basis on the Bloch sphere. The wave plates are controlled by a computer to enable adaptation and driven by two step-motor stages. In order to show the best performance of this adaptive scheme, we take several strategies to reduce the system error as much as possible. To alleviate the drift of the collective efficiency of two photon detectors, multimode fibers fully covered by black plastic bags instead of single-mode fibers are used to collect the coupled photons, which is observed in our laboratory within 0.002 in 16 h. Because of the introduction of multimode fibers we have to set the coincidence window to 1 ns to minimize the random coincidence count so that its error can be ignored, which also helps make sure one photon is detected at a time. More technical details can be found in Refs. [22,26].

First, the true state is reconstructed with a very large number of copies ($N > 1 \times 10^7$) by the traditional maximum likelihood estimation (MLE) method on the $\sigma_x,\sigma_y,\sigma_z$ basis. The reconstructed state is $(r,\theta,\phi) = (0.999,0.0261,2.554)$ in the Bloch sphere. Since the true state we prepared is nearly aligned with one of the three measurement bases, the reconstruction precision of MLE should be high enough for the following experiments. Then we implement our adaptive tomography schemes in the experiments. The angle of wave plates before the beam displacer in the setup is tuned according to the

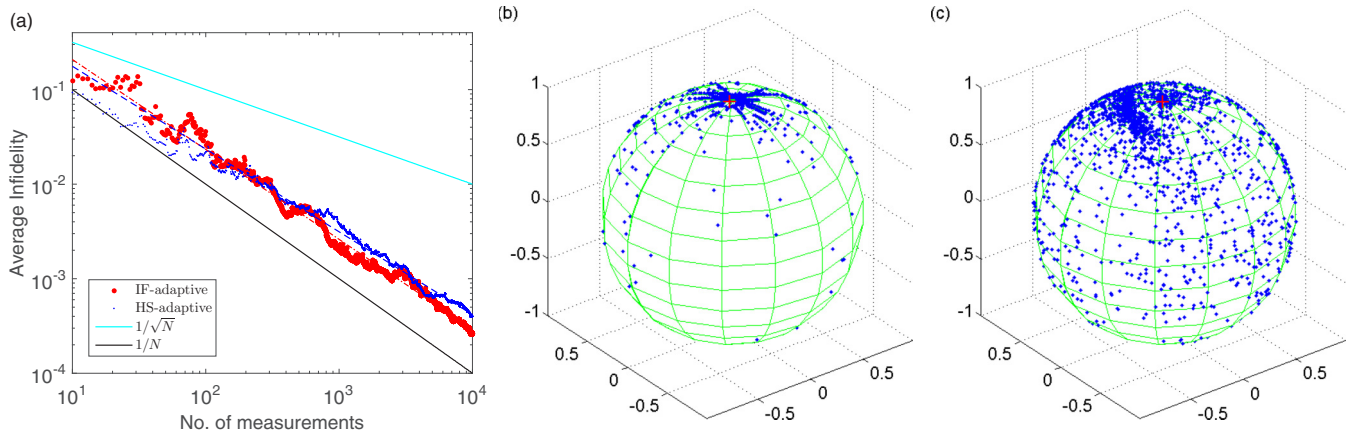

FIG. 3. Experimental results: (a) average infidelity against the number of measurements reconstructed by IF-based (red bold dots) and HS-based (blue tiny dots) adaptive tomography. The red dash-dotted line and blue dashed lines are their fitting results, respectively. The cyan (upper) line of $1 - F = 1/\sqrt{N}$ and black (lower) line of function $1 - F = 1/N$ are shown for comparison. Data points are averaged over 20 experimental runs. (b, c) Distribution of the measurement basis on the Bloch sphere of one of the experimental runs for IF and HS, respectively. These blue dots are one-fifth of the basis sequence chosen with equal interval, and the red plus is the true state.

adaptive program, which computes the next measurement basis each time after the coincidence is observed. As pointed out above, the analytical solution for the one-qubit case is computationally efficient, so our adaptive process is conducted in real time. In fact, the next basis is achieved almost instantly after the measurement feedback in our program even for large N. However, the most time-consuming procedure is to switch the angles of the wave plates, which are controlled by two step-motor stages with high precision but slow speed, resulting in about 4 h for one experimental run of $N = 1 \times 10^4$ measurements.

The estimation infidelity is averaged over 20 experimental runs, and the results are presented in Fig. 3. As expected, we can see from Fig. 3(a) that the decreasing gradients of both IF- and HS-based adaptive tomography are much larger than that of the $1/\sqrt{N}$ scaling rule, while approaching that of the $1/N$ scaling rule. Also IF outperforms HS a bit, as in simulations. The power law of $1 - F \propto 1/N^{\alpha}$ has been fit for all data; we get $\alpha = -0.97 \pm 0.05$ and -0.80 ± 0.05 for IF- and HS-based tomography, respectively, which agrees with the simulation results within error bars. Then we try to discover some details of the measurement basis performed in our experiments. Figures 3(b) and 3(c) show the distribution of the measurement basis of one of the experimental runs on the Bloch sphere for IF- and HS-based tomography, respectively. On the one hand, the measurement basis can be chosen anywhere on the Bloch sphere with certain probability; on the other hand, these bases have a tendency to gather around the true state, which makes it seem that the adaptive schemes guide the basis to the true state. This is kind of similar to the self-guided tomography theme proposed in Ref. [27]. We notice the points of measurement basis of IF-based tomography are much more concentrated around the true state than that of HS-based tomography. Besides, the points in Fig. 3(b) almost cluster along the lines connecting the real state and some early chosen measurement bases. The reason for this feature can be revealed from the update rule. We know from Eq. (4) the next measurement basis is dependent on the previous ones and the true state; usually the early part of measurement bases would be chosen rather randomly due to the little information, then after certain steps the next measurement basis is chosen to minimize the variance. According to Ref. [21], the closer the measurement basis is to the true state, the more accurate the estimation is, so it is reasonable that the measurement basis approaches the true state, and the faster it approaches, the better accuracy you get. Second, the update rule is based on the calculation of the Fisher information, which is summed over the previous measurement basis. We believe that, due to the two above reasons, choosing the measurement basis clustering along the lines is the fast way to improve the accuracy and approximate the quantum Cramér-Rao inequality, which also explains why IF-based adaptive tomography achieves better performance than HS, whose distribution of measurement basis is dispersive.

V. CONCLUSIONS

We have experimentally realized the adaptive quantum-state tomography based on an average-variance optimality criterion in optical system. Both IF- and HS-based tomography outperform traditional nonadaptive methods, achieving almost the $1/N$ scaling rule in terms of average infidelity, which is believed to be the theoretical limit for any tomography scheme [12,13]. And the reason why HS-based tomography behaves a little worse than IF-based tomography has been analyzed through the distribution of its measurement basis on the Bloch sphere in an intuitive way. We notice that the more and the faster the measurement bases cluster around the true state, the better tomography performance is, which agrees with the result of Ref. [21]. With an analytic solution for the one-qubit case, this adaptive scheme overcomes the high-computational-cost problem and enables real-time feedback measurement, so that the number of measurement copies can be much improved with respect to other schemes [16–18], which makes it feasible to implement the adaptive strategy in practical quantum-state tomography experiments. Though

controlling the motion of the wave plates in our experiments is time consuming, that will not be a problem if it is applied in other quantum systems such as ion traps and superconductor circuits, which are measured by laser or microwave [28,29].

ACKNOWLEDGMENTS

We would like to thank Zhibo Hou for helpful discussion and technical support. The work is supported by the National Natural Science Foundation of China (Grants No. 61222504 and No. 11574291).

[1] M. A. Nielsen and I. L. Chuang, *Quantum Computation and Quantum Information* (Cambridge University Press, Cambridge, UK, 2000).

[2] H. Häffner *et al.*, Nature (London) **438**, 643 (2005).

[3] J. L. O'Brien, G. J. Pryde, A. G. White, T. C. Ralph, and D. Branning, Nature (London) **426**, 264 (2003).

[4] D. T. Smithey, M. Beck, M. G. Raymer, and A. Faridani, Phys. Rev. Lett. **70**, 1244 (1993).

[5] Z. Hradil, Phys. Rev. A **55**, R1561 (1997).

[6] D. F. V. James, P. G. Kwiat, W. J. Munro, and A. G. White, Phys. Rev. A **64**, 052312 (2001).

[7] E. Bagan, M. Baig, R. Muñoz-Tapia, and A. Rodriguez, Phys. Rev. A **69**, 010304(R) (2004).

[8] E. Bagan, M. A. Ballester, R. D. Gill, R. Muñoz-Tapia, and O. Romero-Isart, Phys. Rev. Lett. **97**, 130501 (2006).

[9] R. B. A. Adamson and A. M. Steinberg, Phys. Rev. Lett. **105**, 030406 (2010).

[10] M. D. de Burgh, N. K. Langford, A. C. Doherty, and A. Gilchrist, Phys. Rev. A **78**, 052122 (2008).

[11] Yu. I. Bogdanov, G. Brida, I. D. Bukeev, M. Genovese, K. S. Kravtsov, S. P. Kulik, E. V. Moreva, A. A. Soloviev, and A. P. Shurupov, Phys. Rev. A **84**, 042108 (2011).

[12] S. Massar and S. Popescu, Phys. Rev. Lett. **74**, 1259 (1995).

[13] E. Bagan, M. A. Ballester, R. D. Gill, A. Monras, and R. Muñoz-Tapia, Phys. Rev. A **73**, 032301 (2006).

[14] D. G. Fischer, S. H. Kienle, and M. Freyberger, Phys. Rev. A **61**, 032306 (2000).

[15] Th. Hannemann, D. Reiss, Ch. Balzer, W. Neuhauser, P. E. Toschek, and Ch. Wunderlich, Phys. Rev. A **65**, 050303(R) (2002).

[16] A. Fujiwara, J. Phys. A **39**, 12489 (2006).

[17] C. J. Happ and M. Freyberger, Phys. Rev. A **78**, 064303 (2008).

[18] D. G. Fischer and M. Freyberger, Phys. Lett. A **273**, 293 (2000).

[19] T. Sugiyama, P. S. Turner, and M. Murao, Phys. Rev. A **85**, 052107 (2012).

[20] K. S. Kravtsov, S. S. Straupe, I. V. Radchenko, N. M. T. Houlsby, F. Huszár, and S. P. Kulik, Phys. Rev. A **87**, 062122 (2013).

[21] D. H. Mahler, L. A. Rozema, A. Darabi, C. Ferrie, R. Blume-Kohout, and A. M. Steinberg, Phys. Rev. Lett. **111**, 183601 (2013).

[22] Z. B. Hou, H. J. Zhu, G. Y. Xiang, C. F. Li, and G. C. Guo, npj Quantum Inf. **2**, 16001 (2016).

[23] F. Pukelsheim, *Optimal Design of Experiments*, Classics in Applied Mathematics (SIAM, Philadelphia, 2006).

[24] B. Qi, Z. B. Hou, L. Li, D. Y. Dong, G. Y. Xiang, and G. C. Guo, Sci. Rep. **3**, 3496 (2013).

[25] C. R. Rao, *Linear Statistical Inference and Its Applications*, Wiley Series in Probability and Statistics, 2nd ed. (Wiley, New York, 2002).

[26] Z. B. Hou, H. J. Zhu, G. Y. Xiang, C. F. Li, and G. C. Guo, J. Opt. Soc. Am. B **33**, 1256 (2016).

[27] C. Ferrie, Phys. Rev. Lett. **113**, 190404 (2014).

[28] D. Leibfried, R. Blatt, C. Monroe, and D. Wineland, Rev. Mod. Phys. **75**, 281 (2003); D. B. Hume, T. Rosenband, and D. J. Wineland, Phys. Rev. Lett. **99**, 120502 (2007).

[29] Y. Makhlin, G. Schön, and A. Shnirman, Rev. Mod. Phys. **73**, 357 (2001); I. Chiorescu, Y. Nakamura, C. J. P. M. Harmans, and J. E. Mooij, Science **299**, 1869 (2003).